A novel coordinated control algorithm for distributed driving electric vehicles

Shixin Song[1], Wanchen Sun[2], Feng Xiao[2,*], Silun Peng[2], Jingyu An[2], Da Wang[2]

1. College of Mechanical and Engineering, Jilin University, Changchun 130022, China

2. State Key Laboratory of Automotive Simulation and Control, Jilin University, Changchun 130022, China

xiaofeng4206@126.com

ABSTRACT. *This paper combines the electric stability control (ESC) and drive force assisted steering (DFAS) into a novel coordinated control algorithm for distributed driving electric vehicles. Specifically, a correction factor ki was introduced to modify the driving force and fuzzy control rules were designed for different vehicle attitudes and lane change conditions. On this basis, the author determined the basic framework of the coordinated control algorithm. Then, the proposed algorithm was verified through simulation tests and real-vehicle experiments. The results show that the proposed algorithm ensures good stability and steering performance and is feasible for the control of distributed driving electric vehicles.*

RÉSUMÉ. *Dans cet article, le système de contrôle de la stabilité électrique (ESC) et le système de direction assistée par la force motrice (DFAS) sont combinés dans un nouvel algorithme de contrôle coordonné pour les véhicules électriques à conduite distribuée. Plus précisément, un facteur de correction ki a été introduit pour modifier la force motrice et des règles de contrôle floues ont été conçues pour différentes postures des véhicules et conditions de changement de voie. Sur cette base, l'auteur a déterminé le cadre de base de l'algorithme de contrôle coordonné. Ensuite, l'algorithme proposé a été vérifié au moyen de tests de simulation et d'expériences sur des véhicules réels. Les résultats montrent que l'algorithme proposé garantit une bonne stabilité et de bonnes performances de direction et qu'il est réalisable pour le contrôle de véhicules électriques à conduite distribuée.*

KEYWORDS: *vehicle dynamics, distributed driving electric vehicle, electric stability control (ESC), drive force assisted steering (DFAS).*

MOTS-CLÉS: *dynamique du véhicule, véhicule électrique à conduite distribuée, contrôle de stabilité électrique (ESC), direction assistée par la force motrice (DFAS).*

DOI:10.3166/JESA.50.405-421

1. Introduction

Distributed driving electric vehicles mark the future trend of the automotive industry, thanks to their simple structure, greenness and energy efficiency (Murata, 2012). With the proliferation of such vehicles, the stability control has become a research hotspot (Mizushima *et al*., 2006; Esmailzadeh *et al*., 2003). These vehicles realize a high degree of freedom (DOF) and independent control of wheels through the removal of the differential mechanism. The torque distribution of the four wheels is more flexible than that of conventional cars, which enhances the stability control of the vehicle (Zou *et al*., 2009; Sakai and Hori, 2001; Hori, 2004; Ono *et al*., 2006).

During four-wheel independent driving, the electric stability control (ESC) and differential drive assisted steering (DDAS) are realized through the differential motion between the left and right driving wheels. The two operations have similar principles, and may disturb or complement each other under certain circumstances. Recently, the DDAS has been replaced by the drive force assisted steering (DFAS). The new steering method has been explored in great depth by researchers (Wu and Yeh, 2008; Besselink, 2003; Wang *et al.*, 2010).

Considering the above, this paper combines the ESC and the DDAS into a coordinated control algorithm, with the aim to promote the popularization of distributed driving electric vehicles.

2. Coordinated control algorithm

2.1. Basic principles

On vehicle stability control, Shibahata (Jin *et al*., 2004) suggested that a vehicle will loose control if its sideslip angle surpasses 12º on a dry road or 5º on a road with low friction coefficient. Based on wheel motor driving features, Jin and Liu (2014) estimated the kinematic geometry of vehicle yaw speed and sideslip angle, and applied this method to optimize the control of the whole vehicle, revealing that the vehicle stability can be effectively controlled under the proper sideslip angle and yaw speed. Reference (Wang *et al*., 2009) carries out differential calculation of sideslip angle according to the basic parameters acquired by a sensor, and creates a sliding mode variable structure controller.

In the DAFS for four-wheel independent driving, the driving torque on both sides of the wheel can be adjusted as required to generate the torque for assistive steering (Wang *et al*., 2009; Song *et al*., 2013). The nonlinear power can distinguish changes in hand force at the same speed. The greater the hand force, the more assistance power is needed (Liu *et al*., 2013; Ross, 1994). The relationship between the vehicle speed and the steering wheel hand force should be Ta=ka(v)Th2, with ka(v) being the assist coefficient at different speeds and Th being the current hand force of the driver.

2.2. Algorithm design

Since the differential assistance should be adjusted according to the real-time stability, it is necessary to define a correction coefficient ki [0, 1] to modify the boosting feature function Ta=kika(v)Th2. The fuzzy controller was selected to design the coordinated control algorithm, because this controller does not need a controlled object and the control magnitude can be determined by looking up the table of control decisions, which are organized based on the manual control rules. The fuzzy control flow chart is shown in Figure 1, where μ is the tire-road friction coefficient, β is the sideslip angle, and γ is the vehicle yaw speed.

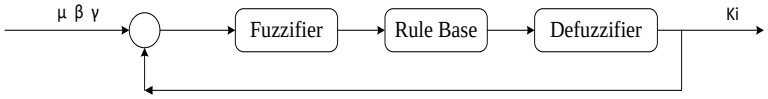

Figure 1. Fuzzy control flow chart

After entering the vehicle sensor, the input signals were processed under fuzzy rules, yielding proper control output signals. Considering the differential features, μ, $|\beta_{ideal}/\beta_{real}|$ and $|\gamma_{ideal}/\gamma_{real}|$ were taken as the inputs. The values of $|\beta_{ideal}/\beta_{real}|$ and $|\gamma_{ideal}/\gamma_{real}|$ are negatively correlated with the tendency of the vehicle to lose stability, and positively with the output power factor. The parameter μ is the adhesion coefficient, which has a certain impact on the output. The fuzzy rules between the parameters are listed in Table 1 below.

Table 1. Fuzzy rules of the parameters

$\lvert\gamma_{ideal}/\gamma_{real}\rvert$	$\lvert\beta_{ideal}/\beta_{real}\rvert$	μ	ki	$\lvert\gamma_{ideal}/\gamma_{real}\rvert$	$\lvert\beta_{ideal}/\beta_{real}\rvert$	μ	ki
PS	*PS*	*PS*	*ZE*	*PM*	*PB*	*PM*	*PM*
PS	*PM*	*PS*	*ZE*	*PB*	*PS*	*PM*	*PM*
PS	*PB*	*PS*	*ZE*	*PB*	*PM*	*PM*	*PB*
PM	*PS*	*PS*	*PS*	*PB*	*PB*	*PM*	*PB*
PM	*PM*	*PS*	*PS*	*PS*	*PS*	*PB*	*ZE*
PM	*PB*	*PS*	*PM*	*PS*	*PM*	*PB*	*ZE*
PB	*PS*	*PS*	*ZE*	*PS*	*PB*	*PB*	*PS*
PB	*PM*	*PS*	*PM*	*PM*	*PS*	*PB*	*PM*
PB	*PB*	*PS*	*PB*	*PM*	*PM*	*PB*	*PB*
PS	*PS*	*PM*	*ZE*	*PM*	*PB*	*PB*	*PB*
PS	*PM*	*PM*	*ZE*	*PB*	*PS*	*PB*	*PB*
PS	*PB*	*PM*	*ZE*	*PB*	*PM*	*PB*	*PB*
PM	*PS*	*PM*	*PS*	*PB*	*PB*	*PB*	*PB*
PM	*PM*	*PM*	*PM*				

The designed process of the coordinated control algorithm is described in Figure

2 below. Firstly, the algorithm determines whether the differential power system is working (i.e. whether △M is 0) according to the current Th and driver hand speed V. If the system is not working, the four motors are only responsible for stability control; If the system is working, the algorithm judges if the differential power generated by the yaw torque of △M is the same as that for the stability control in the yaw torque direction Mc. If yes, the torque needed for stability control is calculated from the basic driving power, and the insufficient amount is compensated by the differential torque of rear wheel △Tr; if not, the ratio of the ideal yaw speed to the actual yaw speed is computed, the ratio of the ideal centroid sideslip angle to the actual centroid sideslip angle is computed, and the current road condition is estimated. After that, the three quantities are imported to the fuzzy controller, which then outputs the correction coefficient ki of the original power assisted function as well as the corresponding driving torque to adjust the power. The adjustment is similar to back-wheel compensation. Owing to the limit on the rear torque, the stability control should be prioritized if the computing time is not sufficient to compensate for rear wheel stability requirements; then, the driving assistance system will stop working, leaving the front and rear wheels to control vehicle stability.

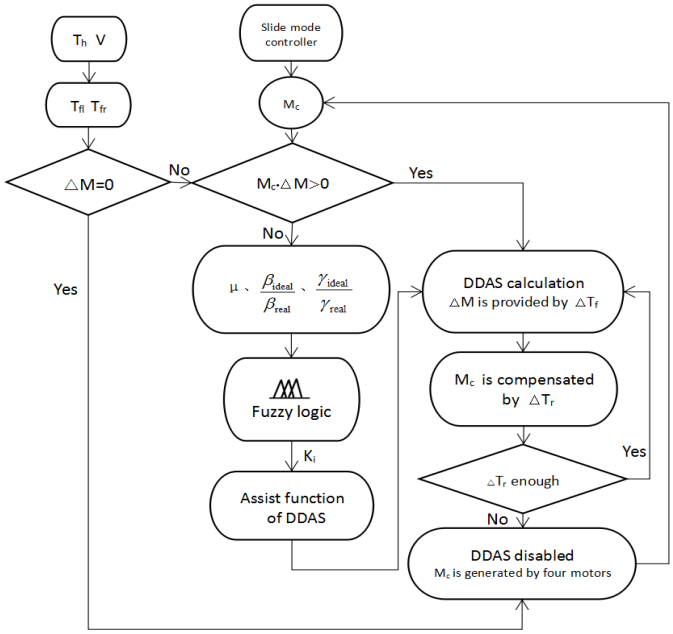

Figure 2. Process of the coordinated control algorithm

3. Design of vehicle dynamics model

Our coordinated controller was developed based on a 3DOF vehicle model and a 2DOF reference model. The estimation of the lateral force of each tire was improved

with a nonlinear tire model. In addition, the parameters were adjusted because the hub motor may increase the unsprung mass of the vehicle. The basic parameters of the vehicle are listed in Table 2 below.

Table 2. Basic parameters of the vehicle

Parameter	Unit	Value	Parameter	Unit	Value
Vehicle length	mm	4660	Ratio of steering gear	null	1:20
Vehicle width	mm	1795	Kingpin inclination angle	deg	3
Vehicle height	mm	1801	Scrub radius	mm	100
Distance between CG and front axle	mm	1110	Kerb mass	kg	1690
Wheel base	mm	2776	Sprung mass	kg	1370
Height of CG	mm	540	Unsprung mass	kg	80
Moment of inertia about x axis	Kg.m^2	606.1	Rolling radius of wheel	mm	330
Moment of inertia about z axis	Kg.m^2	1729	Cornering stiffness	N/deg	70000

3.1. 3DOF vehicle model

The 3DOF vehicle model for controller design is illustrated in Figure 3. This model characterizes the essential dynamic properties of a road vehicle in the longitudinal, lateral and yaw directions.

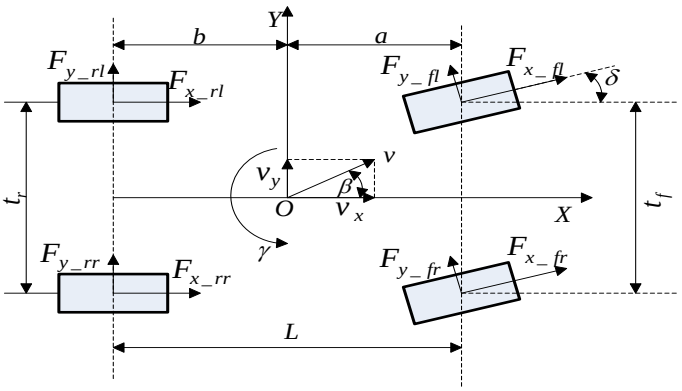

Figure 3. 3DOF vehicle model

The differential equations for longitudinal, lateral and yaw dynamics can be expressed as:

$$a_x = \dot{v}_x - r v_y \tag{1}$$

$$a_y = \dot{v}_y - r v_x \tag{2}$$

$$I_z \dot{\gamma} = M_z \tag{3}$$

$$\begin{aligned} M_z = a(&F_{x\_fl}\sin\delta + F_{y\_fl}\cos\delta + F_{x\_fr}\sin\delta + \\ &F_{y\_fr}\cos\delta) - \frac{t_f}{2}(F_{x\_fr}\cos\delta - F_{y\_fr}\sin\delta - \\ &F_{x\_fl}\cos\delta + F_{y\_fl}\sin\delta) - b\left(F_{y\_rl} + F_{y\_rr}\right) \\ &+ \frac{t_r}{2}(F_{x\_rr} - F_{x\_rl}) \\ = a(&F_{y\_fl}\cos\delta + F_{y\_fr}\cos\delta) - \frac{t_f}{2}(F_{y\_fl}\sin\delta \\ &- F_{y\_fr}\sin\delta) - b\left(F_{y\_rl} + F_{y\_rr}\right) + \Delta M \\ \Delta M = a(&F_{x\_fl}\sin\delta + F_{x\_fr}\sin\delta) - \frac{t_f}{2}(F_{x\_fr}\cos\delta \\ &- F_{x\_fl}\cos\delta) + \frac{t_r}{2}(F_{x\_rr} - F_{x\_rl}) \end{aligned} \tag{4}$$

where v_x is the longitudinal speed of the centroid (m/s); v_y is the lateral speed of the centroid (m/s); γ is the yaw speed (rad/s); a_x is the longitudinal acceleration of the centroid (m/s^2); a_y is the lateral acceleration of the centroid (m/s^2); a and b are the distance between the centroid and the front axle and the rear axle, respectively (m); $t_{f,r}$ is the front and rear wheel track (m); F_{x_ij} is the longitudinal force (N); F_{y_ij} is the lateral force (N); I_z is the moment of inertia about z axis (kgm^2); M_z is the torque about the z axis (Nm); δ is the front wheel steering angle; ij=*fl,fr,rl,rr*. Note that the first subscript in the symbols of the lateral tire force denotes the front or rear wheel and the second subscript denote the left or right wheel.

3.2. 2DOF reference model

To explore the turning behavior, steering response and stability of vehicle, a two-wheel vehicle model, also known as the single-track model or bicycle model, was introduced (Figure 4) under the assumption that the two tires of an axle are equivalent to one substitutive tire in the center plane of the vehicle and that the centroid height of the vehicle is negligible. This model serves as the 2DOF reference model to

approximate the dynamic features of the vehicle.

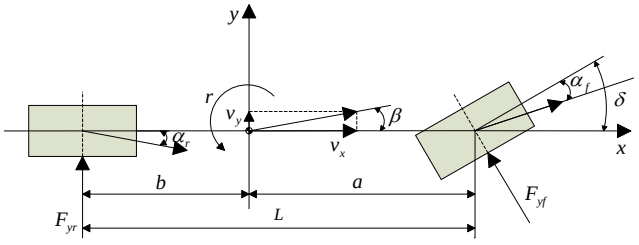

Figure 4. 2DOF reference model

The dynamic equations of the 2-DOF vehicle model can be expressed as:

$$\begin{cases} (C_f + C_r)\beta + \frac{a\,C_f - bC_r}{v_x} \cdot r - C_f\,\delta = mv_x(\dot{\beta} + r) \\ (a\,C_f - bC_r)\beta + \frac{a^2\,C_f + b^2C_r}{v_x} \cdot r - a\,C_f\,\delta = I_z\dot{r} \end{cases} \tag{5}$$

Where β is the vehicle sideslip angle; δ is the front-wheel steering angle; r is the vehicle yaw speed; V_x is the longitudinal speed; V_y is the lateral speed; m is the vehicle mass; a and b are the distance between the centroid and the front axle and that between the centroid and the rear axle, respectively; C_f and C_r are the cornering stiffnesses of the front axle and the rear axle, respectively; I_z is the rotational inertia of the vehicle about the z axis.

Then, the transfer functions can be obtained by Laplace transform:

$$\frac{r}{\delta}(s) = G_r \cdot \frac{\tau_1 + 1}{T_2 s^2 + T_1 s + 1} \tag{6}$$

$$\frac{\beta}{\delta}(s) = G_r \cdot \frac{\tau_1' + 1}{T_2 s^2 + T_1 s + 1} \tag{7}$$

Where $G_r = \frac{v_x}{L \cdot \left(1 + Cv_x^2\right)}$, $G_\beta = \frac{b - mav_x^2 / C_r \cdot L}{L \cdot \left(1 + Cv_x^2\right)}$

Where C is the stability factor: $C = m(aC_f - bC_r) / C_f C_r L^2$

where G_r and G_β are the steady-state gains of the yaw speed and the sideslip angle, respectively.

Then, the ideal yaw speed and the ideal sideslip angle can be described as:

$$\gamma_d = G_r \cdot \delta \tag{8}$$

$$\beta_d = G_\beta \cdot \delta \tag{9}$$

The yaw speed is subjected to the upper bound below:

$$\gamma_{\lim} = 0.85\left|\frac{\mu g}{v_x}\right| \tag{10}$$

Where μ is the tire-road friction coefficient. The desired yaw speed can be defined as:

$$\gamma_{des} = \min\left\{\gamma_d, \gamma_{\lim}\right\} \tag{11}$$

The upper bound for the sideslip angle is recommended as:

$$\beta_{\lim} = \tan^{-1}\left(0.02\mu g\right) \tag{12}$$

The desired sideslip angle of the vehicle can be defined as:

$$\begin{aligned} \beta_{des} &= \beta_d \text{ if } \left|\beta_d\right| \le \beta_{lim} \\ \beta_{des} &= \beta_{lim}\,\mathrm{sgn}\left(\beta_d\right) \text{if } \left|\beta_d\right| \le \beta_{lim} \end{aligned} \tag{13}$$

3.3. Rotational dynamics of the wheels

The rotational dynamics of the four wheels can be described by the following torque balance equation:

$$\left(F_{x\_ij} + F_{z\_ij} f_{ij}\right) r_{ij} = T_{ij} - J_{ij}\,\dot{\omega}_{ij} \tag{14}$$

where T_{ij} is the drive/brake torque transmitted to a wheel; J_{ij} is the rotational inertia; ω_{ij} is the speed of a wheel; F_{z_ij} is the vertical force on a wheel; f_{ij} is the rolling resistance coefficient; r_{ij} is the effective rolling radius of a wheel. Hence, the longitudinal force can be expressed as:

$$F_{x\_ij} = \frac{1}{r}\left(T_{ij} - J_{ij}\,\dot{\omega}_{ij}\right) - F_{z\_ij} f_{ij} \tag{15}$$

The vertical force can be written as:

$$\begin{cases} F_{z\_fl} = M\left(g\frac{a}{2l} - a_x\frac{h_g}{2l} - a_y\frac{h_g b}{t_f l}\right) \\ F_{z\_fr} = M\left(g\frac{b}{2l} - a_x\frac{h_g}{2l} - a_y\frac{h_g b}{t_f l}\right) \\ F_{z\_rl} = M\left(g\frac{a}{2l} + a_x\frac{h_g}{2l} - a_y\frac{h_g b}{t_f l}\right) \\ F_{z\_rr} = M\left(g\frac{b}{2l} + a_x\frac{h_g}{2l} + a_y\frac{h_g b}{t_f l}\right) \end{cases} \tag{16}$$

where h_g is the height of the vehicle centroid.

3.4. Lateral tire force model

The Dugoff tire model was adopted to calculates of tire lateral force. Here, the calculation formula can be expressed as:

$$F_{y\_ij} = -C_{ij}\tan\alpha_{ij} f(\lambda) \tag{17}$$

where C_{ij} is the cornering stiffness of each tire; μ is the tire-road friction coefficient; λ is given by:

$$\lambda = \frac{\mu F_{z\_ij}}{2C_{ij}|tan\,\alpha_{i,j}|},\ f(\lambda) = \begin{cases} (2-\lambda)\lambda, & if\ \ \lambda < 1 \\ 1\ \ , & if\ \ \lambda \geq 1 \end{cases};$$

α_{ij} are the sideslip angles at the front and rear tires:

$$\alpha_{fl,fr} = -\left(\delta\ \ - arctan\left(\frac{v_y + a\gamma}{v_x \mp \frac{t_f}{2}\gamma}\right)\right),\ \alpha_{rl,rr} = arctan\left(\frac{v_y - b\gamma}{v_x \mp \frac{t_r}{2}\gamma}\right)$$

The tire cornering stiffness depends on the tire load and the load transfer effect on the cornering stiffness. It can be expressed as a second-order polynomial:

$$C_{y\_ij}(F_z) = (mF_{z\_ij} - nF^2{}_{z\_ij}) \tag{18}$$

where m and n are the coefficients in the polynomial. In the modified Dugoff tire model, the C_{ij} is replaced with C_{y_ij}.

4. Simulation verification

To verify the proposed coordinated control algorithm, three simulation tests were carried out under different operating conditions.

In the first simulation test, the vehicle travelled on a road (μ=*0.9*) at a constant speed of 50km/h and made a double lane change. The double lane change was designed according to the *Controllability and Stability Test Procedure for Automobile*

(GB/T 6323-2014), with the aim to simulate the deriver's ability to make overtaking decisions at low and high speeds, which can verify the stability and low-speed power performance of our algorithm.

The simulation results are presented in Figures 5~8. Comparing Figures 5 and 6, it can be seen that, under the coordinated control, the front wheels acted as the steering wheel, leading to a motor torque difference between left and right wheels and even a negative electromagnetic torque on the rear wheels. As shown in Figures 7 and 8, the steering wheel angle varied with the hand force in the double lane change, and the hand force was reduced by 30% at the most. In this way, the driver can operate the vehicle more easily and avoid obstacles more accurately. Thus, the rear wheels can compensate for the front wheels in a coordinated manner when the vehicle moves at a low speed.

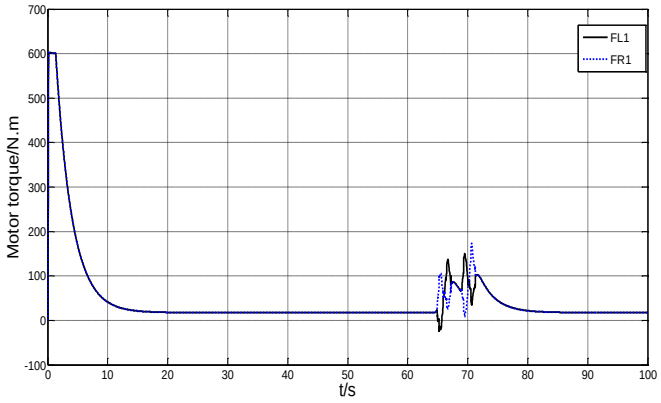

Figure 5. Comparison of front motor torque

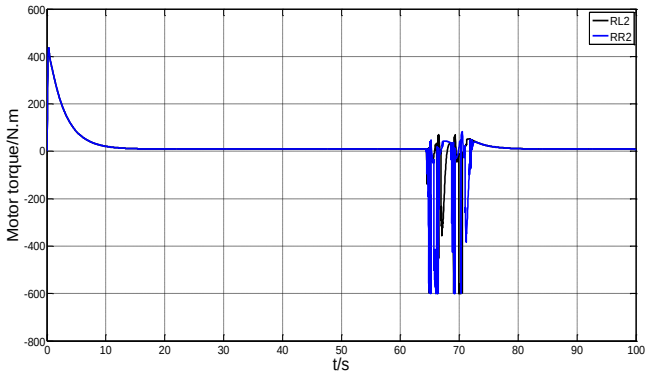

Figure 6. Comparison of rear motor torque

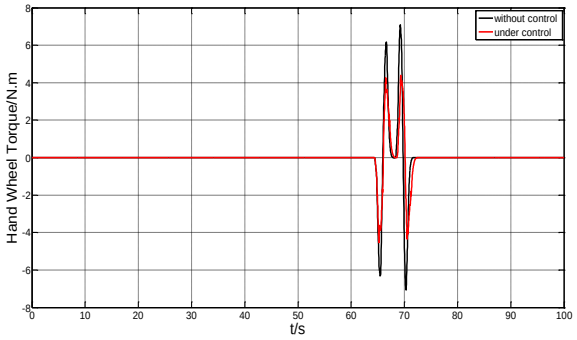

Figure 7. Comparison of steering wheel force

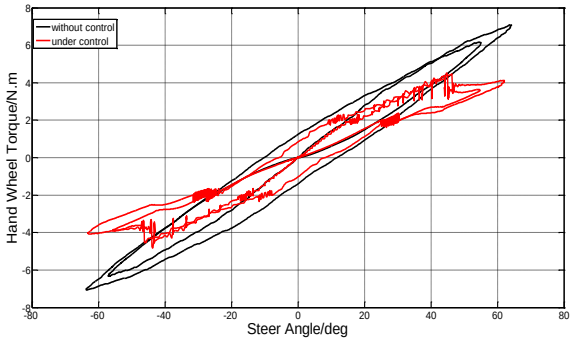

Figure 8. Comparison of the hysteresis curve of steering wheel force

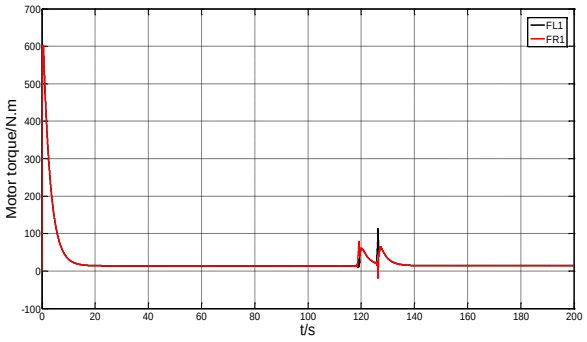

Figure 9. Comparison of front motor torque

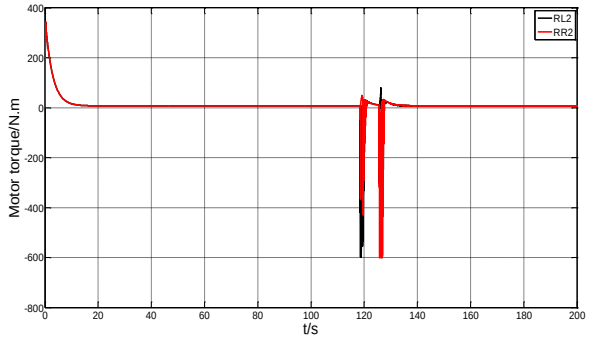

Figure 10. Comparison of rear motor torque

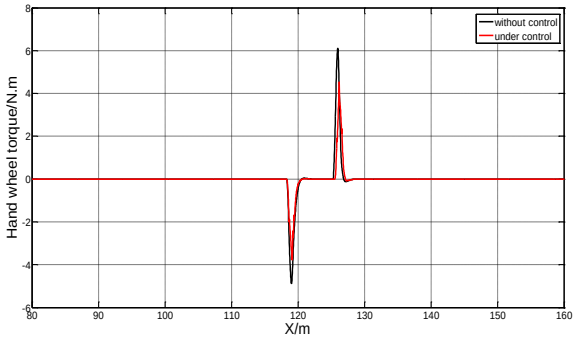

Figure 11. Comparison of steering wheel force

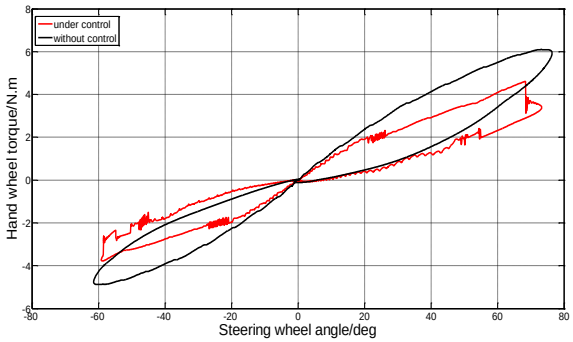

Figure 12. Comparison of the hysteresis curve of steering wheel force

In the second test, the vehicle travelled on the same road at constant speed of 40km/h and made a single lane change. The simulation at low speeds mainly investigates the line capacity. The simulation results are displayed in Figures 9~12. From Figures 9 and 10, it can be seen that the two front wheels are designed to assist the driver in turns, while the two rear wheels are for stability compensation. As shown in Figures 11 and 12, the steering wheel force was reduced by our control algorithm about 30%, fulfilling the requirements on stability and power performance.

In the third test, the vehicle travelled on the same road and made a J-turn. The test is to simulate the vehicle power and stability under the working conditions in a sharp turn. The vehicle speed was designed as V=30km/h. After the acceleration was completed, the steering wheel remained at 180° after 1s. The simulation results are recorded in Figures 13 and 14.

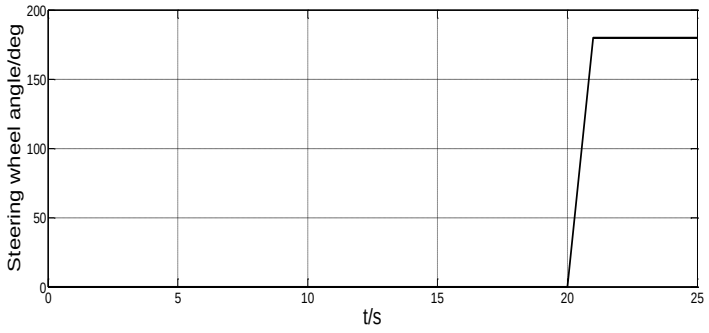

Figure 13. Comparison of the angle input of steering wheel

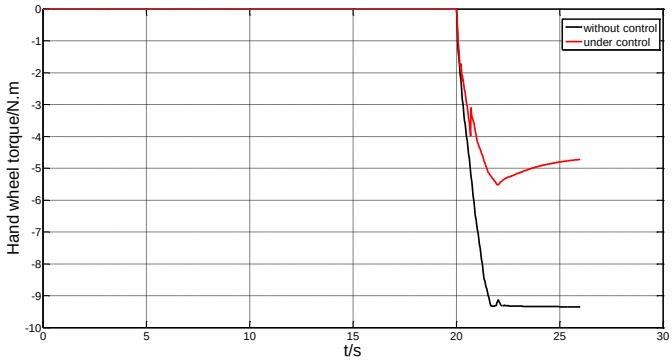

Figure 14. Comparison of steering wheel force

Figure 13 compares the angle input of the steering wheel and Figure 14 compares the hand force of the steering wheel. It can be seen from the two figures that the

proposed control algorithm reduced the hand force by almost 50%, thus easing the driver's workload in sharp turns.

5. Experimental verification

In this section, a distributed driving electric vehicle is built to test the correctness of the coordinated control algorithm. Then, the vehicle was applied to a double-lane change test with the aid of dSPACE MicroAutoBox. The test results are shown in Figures 15~18. From Figures 15 and 16, it can be seen that the proposed algorithm reduced the hand force of the steering wheel. From the 8s, the left and right hub motors started to produce differential torque, leading to vehicle instability. The vehicle was particularly unstable in 7~9s and 12~14s, as the differential torque changed violently at the change points. Then, the rear wheels reacted to ensure the vehicle stability through differential torque compensation. It can be seen from Figure 17 that the control algorithm reduced the yaw speed and the reduction peaked at about 50% at 9.5s and 14.5s. The steering wheel force curve in Figure 18 reveals that the proposed algorithm struck a good balance between stability and power.

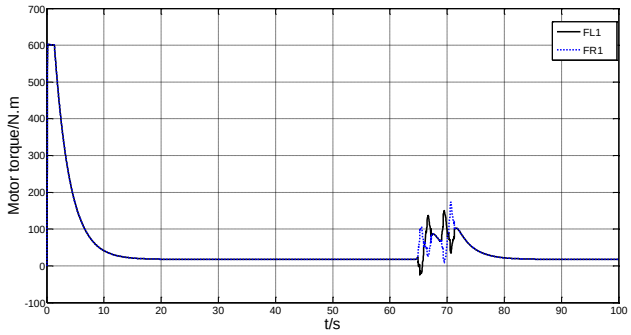

Figure 15. Comparison of front motor torque

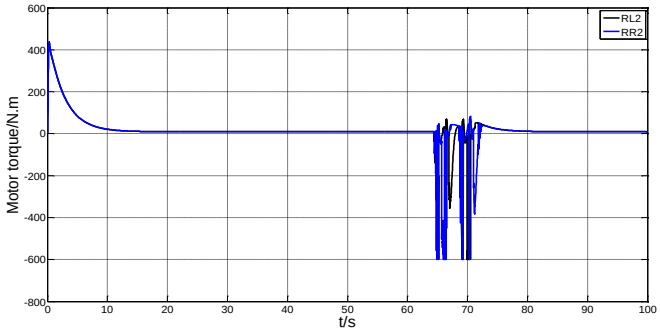

Figure 16. Comparison of rear motor torque

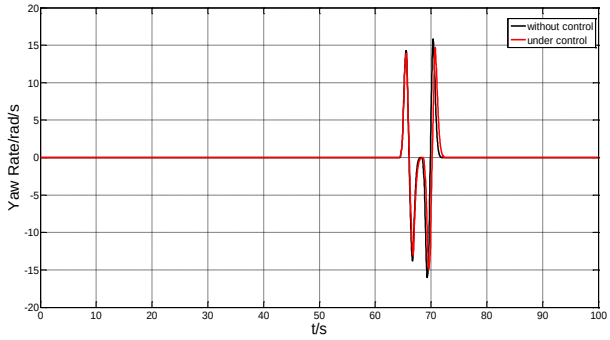

Figure 17. Comparison of yaw speed

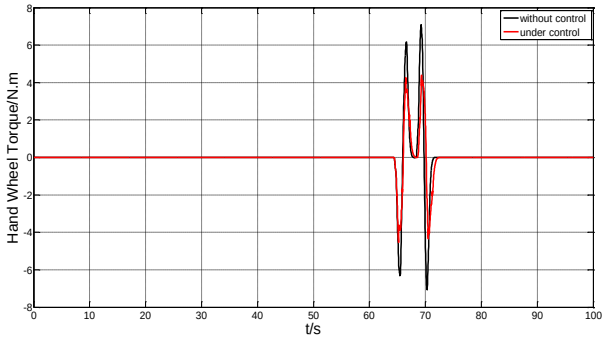

Figure 18. Comparison of the steering wheel force

6. Conclusions

The structure of distributed driving electric vehicles could enhance the effect of vehicle stability control system. In light of this feature, this paper designs a coordinated control strategy based on the ESC and the DFAS systems, and verifies the strategy through simulation and experiments. The simulation and experimental results prove that the control strategy can realize stable control despite power interferences, through the control of the differential torque moment of the front and rear wheels. Under the premise of vehicle stability, our strategy reduces the steering power and hand force, and compensates the insufficient torque by the differential torque on the rear wheels. In addition, our strategy can ensure the vehicle stability and power performance through the coordination between front and rear wheels, when the driving power stops operation under the limit on the rear wheel torque.

Acknowledgments

This work is supported by National Natural Science Foundation of Jilin (No. 20150101037JC).

References

Besselink B. C. (2003). Computer controlled steering system for vehicles having two independently driven wheels. *Computers and Electronics in Agriculture*, Vol. 39, No. 3, pp. 209-226. https://doi.org/10.1016/S0168-1699(03)00081-4

Esmailzadeh E., Goodarzi A., Vossoughi G. R. (2003). Optimal yaw moment control law for improved vehicle handling. *Mechatronics*, Vol. 13, No. 7, pp 659-675. https://doi.org/10.1016/S0957-4158(02)00036-3

Hori Y. (2004). Future vehicle driven by electricity and control-research on four-wheel-motored "UOT electric march II". *IEEE Transactions on Industrial Electronics (S0278-0046)*, Vol. 51, No. 5, pp. 954-962. http://dx.doi.org/10.1109/AMC.2002.1026883

Jin L., Liu Y. (2014). Study on adaptive slid mode controller for improving handling stability of motorized electric vehicles. *Mathematical Problems in Engineering*, Vol. 2014, No. 1, pp. 1-10. https://doi.org/10.1155/2014/240857

Jin L., Wang Q., Song C. (2004). Simulation of 4-wheel independent driving electric vehicle dynamics control system. *Journal of Jilin University (Engineering and Technology Edition)*, Vol. 34, No. 4, pp. 547-553.

Liu Y., Jin L. Q., Liang X. L., Zheng Z. A. (2013). Research on BP based fuzzy-PID controller for anti-lock braking system. *Applied Mechanics and Materials*, Vol. 365-366, pp. 401-406. http://dx.doi.org/10.4028/www.scientific.net/AMM.365-366.401

Mizushima T., Raksincharoensak P., Nagai M. (2006). Direct yaw-moment control adapted to driver behavior recognition. *SICE-ICASE International Joint Conference*, pp. 534-539. http://dx.doi.org/10.1109/SICE.2006.315542

Murata S. (2012). Innovation by in-wheel-motor drive unit. *International Journal of Vehicle Mechanics and Mobility*, Vol. 50, No. 6, pp. 807-830. https://doi.org/10.1080/00423114.2012.666354

Ono E., Hattori Y., Muragishi Y., Koibuchi K. (2006). Vehicle dynamics integrated control for four-wheel-distributed steering and four-wheel-distributed traction/braking system. *Vehicle System Dynamics*, Vol. 44, No. 2, pp. 139-151. https://doi.org/10.1080/00423110500385790

Ross T. J. (1994). Fuzzy Control Systems. *CRC Press*.

Sakai S., Hori Y. (2001). Advanced motion control of electric vehicle with fast minor feedback loops: basic experiments using the 4-wheel motored EV "UOT Electric March II". *JSAE Review (S0389-4304)*, Vol. 22, No. 4, pp. 527-536. https://doi.org/10.1016/S0389-4304(01)00140-0

Song C. X., Xiao F., Jin L. Q., Song S. X., Li J. H., Peng S. L. (2013). Study of modeling and simulation on driving force power steering for electric vehicle with in-wheel-motor-drive. *Applied Mechanics & Materials*, Vol. 13, No. 4, pp. 511-516. http://dx.doi.org/10.4028/www.scientific.net/AMM.397-400.511

Wang J. N., Wang Q. N., Song C. X., Jin L., Hu C. (2010). Co-simulation and test of differential drive assist steering control system for four-wheel electric vehicle. *Transactions of the Chinese Society for Agricultural Machinery*, Vol. 41, No. 6, pp. 7-13. Http://dx.chinadoi.cn/10.3969/j.issn.1000-1298.2010.06.002

Wang Q., Wang J., Jin L., Hu C., Zhang X. (2009). Differential assisted steering applied on electric vehicle with electric motored wheels. *Journal of Jilin University (Engineering and Technology Edition)*, Vol. 39, No. 1, pp. 3-8.

Wang Q., Wang J., Song S. (2009). Validation of differential drive assisted steering system by off-line simulation. *Automotive Engineering*, Vol. 31, No. 6, pp. 545-551. https://doi.org/10.1109/CLEOE-EQEC.2009.5194697

Wu F., Yeh T. J. (2008). A control strategy for an electrical vehicle using two in-wheel motors and steering mechanism. *Proceedings of AVEC*, Vol. 8, pp. 545-551.

Zou G., Lou Y., Li K. (2009). Tire longitudinal force optimization distribution for independent 4WD EV. *Tsinghua University, Sci & Tech*, Vol. 49, No. 5, pp. 719-722, 727.